

# Estimating photometric redshifts with artificial neural networks

Andrew E. Firth<sup>1</sup>, Ofer Lahav<sup>1\*</sup>, Rachel S. Somerville<sup>1,2</sup>

<sup>1</sup> *Institute of Astronomy, University of Cambridge, Cambridge, CB3 0HA, UK*

<sup>2</sup> *Department of Astronomy, University of Michigan, Ann Arbor, MI48109–1090, USA*

Submitted to MNRAS, 15 March 2002

## ABSTRACT

A new approach to estimating photometric redshifts – using Artificial Neural Networks (ANNs) – is investigated. Unlike the standard template-fitting photometric redshift technique, a large spectroscopically-identified training set is required but, where one is available, ANNs produce photometric redshift accuracies at least as good as and often better than the template-fitting method. The Bayesian priors on the underlying redshift distribution are automatically taken into account. Furthermore, inputs other than galaxy colours – such as morphology, angular size and surface brightness – may be easily incorporated, and their utility assessed.

Different ANN architectures are tested on a semi-analytic model galaxy catalogue and the results are compared with the template-fitting method. Finally the method is tested on a sample of 23000 galaxies from the Sloan Digital Sky Survey. The r.m.s. redshift error in the range  $z \lesssim 0.3$  is  $\sigma_z \sim 0.022$ .

**Key words:** surveys – galaxies: distances and redshifts – methods: data analysis

## 1 INTRODUCTION

The basic photometric redshift technique is to use the colours of a galaxy in a selection of medium- or broad-band filters as a crude approximation of the galaxy’s spectral energy distribution or SED, in order to find its redshift and spectral type. The technique is very efficient compared with spectroscopic redshifts since the signal-to-noise in broad-band filters is much greater than the signal-to-noise in a dispersed spectrum and, furthermore, a whole field of galaxies may be imaged at once while spectroscopy is limited to individual galaxies or those that can be positioned on slits or fibres. However photometric redshifts are only approximate at best and are sometimes subject to complete misidentifications. For many applications though, large sample sizes are more important than precise redshifts and photometric redshifts may be used to good effect.

Photometric redshifts date back to Baum (1962; see also Hogg et al. 1998; Weymann et al. 1999). They have been used extensively in recent years on the ultra-deep and well-calibrated Hubble Deep Field observations (e.g. Gwyn & Hartwick 1996; Connolly, Szalay & Brunner 1998; Fernández-Soto, Lanzetta & Yahil 1999; Fontana et al. 2000; Fernández-Soto et al. 2001; Massarotti, Iovino & Buzzoni 2001a; Massarotti et al. 2001b). The most commonly used

approach is the template-fitting technique. This involves compiling a library of template spectra – either theoretical SEDs from population synthesis models (e.g. GISSEL – Bruzual & Charlot 1993) or empirical SEDs (e.g. Coleman, Wu & Weedman 1980). Then the expected flux through each survey filter is calculated for each template SED on a grid of redshifts, with corrections for ISM, IGM and Galactic extinction where necessary. A redshift and spectral type are estimated for each observed galaxy by minimizing  $\chi^2$  with respect to redshift,  $z$ , and spectral type, SED, where

$$\chi^2(z, \text{SED}) = \sum_i \left( \frac{f_i - \alpha(z, \text{SED})t_i(z, \text{SED})}{\sigma_i} \right)^2, \quad (1)$$

$f_i$  is the observed flux in filter  $i$ ,  $\sigma_i$  is the error in  $f_i$ ,  $t_i(z, \text{SED})$  is the flux in filter  $i$  for the template SED at redshift  $z$  and  $\alpha(z, \text{SED})$  (the scaling factor normalizing the template to the observed flux) is determined by minimizing equation 1 with respect to  $\alpha$ , giving

$$\alpha(z, \text{SED}) = \left( \sum_i \frac{f_i t_i(z, \text{SED})}{\sigma_i^2} \right) / \left( \sum_i \frac{t_i(z, \text{SED})^2}{\sigma_i^2} \right). \quad (2)$$

The template-fitting photometric redshift technique makes use of the available and reasonably detailed knowledge of galaxy SEDs and in principle it may be used reliably even for populations of galaxies for which there are few or no spectroscopically confirmed redshifts. However, cru-

\* lahav@ast.cam.ac.uk

cial to its success, is the compilation of a library of accurate and representative template SEDs (see e.g. Hogg et al. 1998; Firth 2002). Empirical templates are typically derived from nearby bright galaxies, which may not be truly representative of high redshift galaxies. Conversely, while theoretical SEDs can cover a large range of star formation histories, metallicities, dust extinction models etc., not all combinations of these parameters (at any particular redshift) are realistic, and the ad hoc inclusion of superfluous templates increases the potential for misidentifications when using observations with noisy photometry.

An alternative approach can be used when one has a sufficiently large (e.g.  $\sim 100$ – $1000$ , depending on the redshift range) and representative subsample with spectroscopic redshifts. Then one can fit a polynomial or other function mapping the photometric data to the known redshifts and use this to estimate redshifts for the remainder of the sample with unknown redshifts (e.g. Connolly et al. 1995b; Brunner, Szalay & Connolly 2000; Sowards-Emmerd et al. 2000). With this approach, errors in the estimated redshifts may also be estimated analytically or via Monte Carlo simulations.

An extension of the latter approach is to use Artificial Neural Networks (ANNs hereafter). ANNs have been used before in astronomy for, amongst other things, galaxy morphological classification (e.g. Storrie-Lombardi et al. 1992; Lahav et al. 1996), morphological star/galaxy separation (e.g. Bertin & Arnouts 1996; Andreon et al. 2000) and stellar spectral classification (e.g. Bailer-Jones, Irwin & von Hippel 1998; Allende Prieto et al. 2000; Weaver 2000). Essentially an ANN takes a set of inputs (e.g. logarithms of fluxes – i.e. magnitudes – in different filters) for each object, applies some non-linear function, and outputs a value (e.g. the estimated redshift). The ANN is first trained – i.e. the coefficients (weights) of the function are optimized – by using a training set where the desired output is known. The ANN may then be used on any number of other objects with similar inputs (i.e. magnitudes in the same filter set) but unknown outputs (i.e. redshifts).

As well as using all of the information contained in the magnitudes and colours, provided the training set is a representative subsample of the data, the ANN will also take into account the Bayesian priors on the galaxy redshift distribution (cf. Benitez 1998; Teplitz et al. 2001). While choosing a template library that is both sufficient and non-superfluous is a source of concern for the template-fitting method, ANNs automatically fit the true range of galaxy SEDs. Another potential advantage of ANNs relative to the template-fitting method is that the weights applied to each filter may be more optimal than simple  $\chi^2$ -weighting. It is interesting then to see how the two methods compare.

The layout of this paper is as follows. In §2 the ANNs are described and in §3 a semi-analytic model (used to provide mock galaxy catalogues) is introduced. In §4 different ANN architectures are compared using the mock galaxy catalogues and in §5 the performance of the ANNs is compared with the performance of the traditional template-fitting method using simulated observations. In §6 the ANNs are tested on Sloan Digital Sky Survey observational data. Finally §7 summarizes the conclusions.

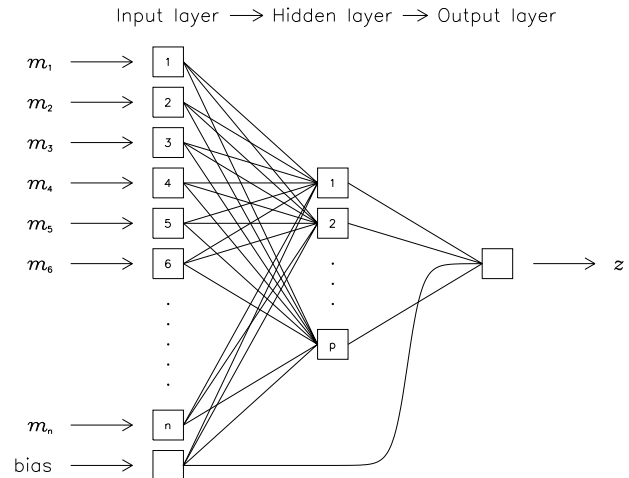


**Figure 1.** A schematic diagram of an ANN with input nodes taking, for example, magnitudes  $m_i = -2.5 \log_{10} f_i$  in various filters, a single hidden layer, and a single output node giving, for example, redshift  $z$ . The architecture is  $n:p:1$  in the notation used in this section. Each connecting line carries a weight  $w_j$ . The bias node allows for an additive constant in the network function defined at each node. More complex nets can have additional hidden layers.

## 2 ARTIFICIAL NEURAL NETWORKS

Following Lahav et al. (1996), an ANN comprises a set of input nodes, one or more output nodes, and one or more hidden layers each containing a number of nodes (Fig. 1). A particular network architecture may be denoted by  $N_{\text{in}}:N_1:N_2:\dots:N_{\text{out}}$  where  $N_{\text{in}}$  is the number of input nodes,  $N_1$  is the number of nodes in the first hidden layer, and so on. For example  $9:6:1$  takes 9 inputs, has 6 nodes in a single hidden layer and gives a single output. The nodes are connected and each connection carries a weight which together comprise the vector of coefficients  $\mathbf{w}$  which are to be optimized. Unless otherwise stated, here every node is assumed to be connected to every node in the previous layer and to every node in the next layer only, but it is certainly possible to have more or less interconnected nets. The input parameters for each object are represented by the vector  $\mathbf{x}$  (e.g. the magnitudes in a set of filters). Given a training set of inputs  $\mathbf{x}_k$  and desired outputs  $z_k$  (e.g. the redshift), the ANN is optimized by minimizing the cost function

$$E = \frac{1}{2} \sum_k [z_k - F(\mathbf{w}, \mathbf{x}_k)]^2. \quad (3)$$

The function  $F(\mathbf{w}, \mathbf{x}_k)$  is given by the network. A function  $g_p$  is defined at each node  $p$ , taking as its argument

$$u_p = \sum_j w_j x_j \quad (4)$$

where the sum is over the input nodes to  $p$ . These functions are typically taken (in analogy to biological neurons) to be sigmoid functions such as  $g_p(u_p) = 1/[1 + \exp(-u_p)]$  (used here). An extra input node – the bias node – is automatically included to allow for additive constants in these functions. The combination of these functions over all the network nodes makes up the function  $F$ . A programme kindly

provided by B. D. Ripley was used to train the networks. The programme takes as its input a network architecture, a training set and a random seed to initiate the weight vector  $\mathbf{w}$ , and uses an iterative quasi-Newton method (see Lahav et al. 1996 for details) to minimize the cost function. To ensure that the weights are regularized (i.e. that they do not become too large), an extra quadratic cost term

$$E_w = \beta \frac{1}{2} \sum_j w_j^2, \quad (5)$$

with  $\beta$  set to 0.001, was added to equation 3. The ideal number of training iterations may be estimated by evaluating the cost function on a separate validation set after each training iteration. This is useful to avoid over-fitting to the training set if the training set is relatively small. For the ANNs investigated in this paper, over-fitting was generally not a problem and the number of training iterations was usually limited to 200 for convenience. Running more training iterations (e.g. 500) typically produces improvements of up to 20 per cent (depending on the network architecture and initial random seed) and should be done for science applications.

### 3 MODEL GALAXY CATALOGUES

To provide a galaxy catalogue on which to train and test ANNs, a semi-analytic model was used. Semi-analytic models are an attempt to use simple recipes to parametrize the main physical processes of galaxy formation within the hierarchical paradigm of galaxy formation (e.g. Kauffmann, White & Guiderdoni 1993; Cole et al. 1994). In these models, Monte Carlo techniques may be used to efficiently generate large mock galaxy catalogues with a (broadly-speaking) realistic distribution of galaxy types, luminosities, colours and redshifts. Here the current version of the code developed by Somerville (1997) is used. This has been shown to produce good agreement with many properties of local and high-redshift galaxies (Somerville & Primack 1999; Somerville, Primack & Faber 2001; Firth et al. 2001).

In this model (see Somerville & Primack 1999 for details), the number density of haloes of various masses at a given redshift is determined by an improved version of the Press-Schechter model (Sheth & Tormen 1999) and the formation and merging of dark matter haloes as a function of time is represented by a ‘merger tree’. The cooling of gas, formation of stars, and reheating and ejection of gas by supernovae within these haloes are modelled by simple recipes. Cold gas is assumed to initially cool into, and form stars within, a rotationally supported disc. Major mergers between galaxies destroy the discs and create spheroids. Galaxy mergers also produce bursts of star formation. The chemical evolution and star formation history of each galaxy is traced and convolved with multi-metallicity stellar population synthesis models (Devriendt, Guiderdoni & Sadat 1999), and a dust extinction law, in order to calculate the galaxy’s SED.

There are several advantages in using a semi-analytic model here. Firstly, an arbitrarily large number of galaxies may be generated over any desired redshift range, and with any magnitude limit. The ‘true’ redshift and magnitudes (prior to the addition of photometric noise) are known

**Table 1.** The mean and r.m.s. in  $\Delta z = z_{\text{model}} - z_{\text{phot}}$  for two networks initialized with different random seeds. A 9:6:1 network architecture and a training set of size 10000 were used. The number of training iterations  $N_{\text{iter}}$  was 200 or 500 as indicated.

$N_{\text{iter}}$	set	random seed 1		random seed 2	
		mean	r.m.s.	mean	r.m.s.
200	training	-0.001	0.089	-0.002	0.102
	testing	-0.004	0.088	-0.006	0.105
500	testing	-0.005	0.087	-0.005	0.089

precisely. At present there is no large observed spectroscopic sample at  $z \gtrsim 0.3$ , and those spectroscopic samples that do exist tend to be biased towards luminous galaxies with prominent emission lines at optical wavelengths. On the other hand, simpler model galaxy catalogues (e.g. PLE models) are less likely to produce realistic distributions of galaxy SEDs in terms of composite stellar populations, ages, metallicities and the effects of dust (all as a function of redshift). Where (when) suitable spectroscopic samples exist, the model catalogues could be replaced by observed photometric and spectroscopic samples and the results would be expected to be comparable (see e.g. §6).

### 4 COMPARING NETWORK ARCHITECTURES

To begin with, an  $H < 22$  semi-analytic model catalogue in *UBVRIZJHK*, with no photometric noise, was used to compare various architectures, training set sizes and the number of training iterations. The magnitudes in each filter and the model redshifts were all normalized to the range  $[0, 1]$  so that all weights are treated fairly equally in equation 5. For definiteness, in each filter the mean magnitude (derived from the training set) was subtracted and the range  $[-5, 5]$  was mapped linearly to  $[0, 1]$ , while the redshift range  $[0, 3.5]$  was also mapped linearly to  $[0, 1]$ . This accounted for essentially all of the galaxies in the sample.

First of all, the stability with respect to different random seeds (for choosing initial weights) was investigated. A 9:6:1 network architecture was used and the ANN was trained on a sample of size 10000 (the training set) with 200 iterations. The completed ANN was tested on a separate sample of size 2000 (the testing set). Note that the testing set could be any size. A sample of size 2000 was chosen simply to provide good statistics. Table 1 tabulates the results, measured by the mean and r.m.s. in  $\Delta z = z_{\text{model}} - z_{\text{phot}}$ , where  $z_{\text{phot}}$  is the ANN photometric redshift. Not surprisingly the results are slightly better when the ANN is run on the training set than when it is run on the separate testing set, but the difference is very small. Fig. 2 compares the estimated photometric redshifts on the testing set for the two random seeds. The different random seeds produce r.m.s. that differ by 15 per cent. However if 500 training iterations are used, the two r.m.s. values begin to converge (0.087 and 0.089 respectively).

Several other networks were investigated using the  $H < 22$  noiseless *UBVRIZJHK* catalogue. Further networks were investigated using just *UBVRIH* as inputs, since this substantially reduces the size of the networks and hence re-

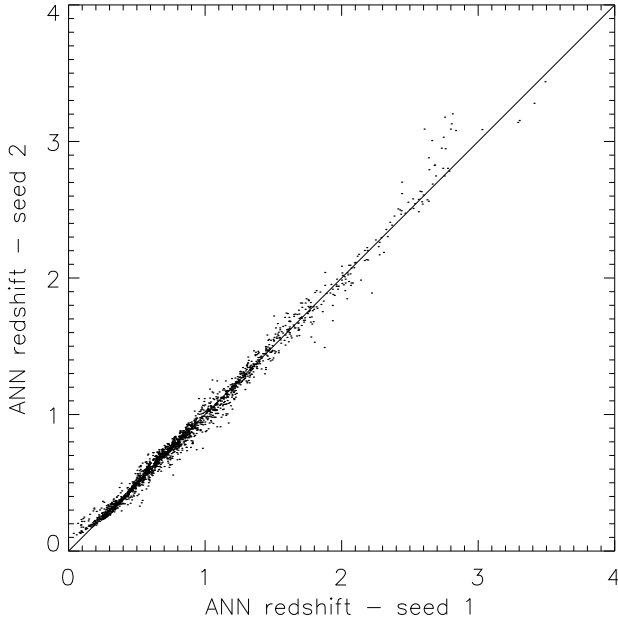


**Figure 2.** Comparison of photometric redshifts on the testing set for two ANNs initialized with different random seeds. A 9:6:1 network architecture, a training set of size 10000 and 200 training iterations were used.

duces the processing time. The results for various architectures, training set sizes and number of training iterations are displayed in Table 2. The architectures 9:6:1 and 9:3:1 obtained r.m.s. in  $\Delta_z$  as low as 0.09 and 0.13 respectively while the architectures 6:3:1, 6:6:1, 6:13:6:13:1, 6:3:3:1 and 6:3:3:1\* (the latter with all possible inter-layer connections rather than just connections between consecutive layers) obtained r.m.s. as low as 0.16, 0.12, 0.09, 0.12 and 0.10 respectively, all with a training set of size 10000 and 200 training iterations. Increasing the number of training iterations or the training set size decreases the r.m.s. obtained, but only up to a certain point. For example the 9:6:1 net is substantially worse, in terms of r.m.s., if only 100 training iterations or a training set of size 5000 is used, but there is little further improvement on a training set of size 10000 and 200 training iterations if the number of iterations is increased to 400 or the training set size is increased to 20000. The number of weights to be fitted increases rapidly with the number of nodes and consequently more complex nets require more training iterations and/or larger training set sizes to approach the optimal r.m.s.. With a training set of size 50000 and 500 training iterations, the 6:13:6:13:1 architecture achieves an r.m.s. of 0.07. However, even for a fixed training set size and number of training iterations, the more complex nets provide better results (clearly this might break down when the number of weights approaches the training set size but that does not occur here). In view of applying the method to real data, one can still do fairly well with much smaller training sets; for example an r.m.s. of 0.14 is achieved with the 9:6:1 architecture with a training set of only 1000 galaxies. Fig. 3 compares estimated and model redshifts for several of these ANNs.

## 5 ASSESSING NEURAL NETWORKS WITH

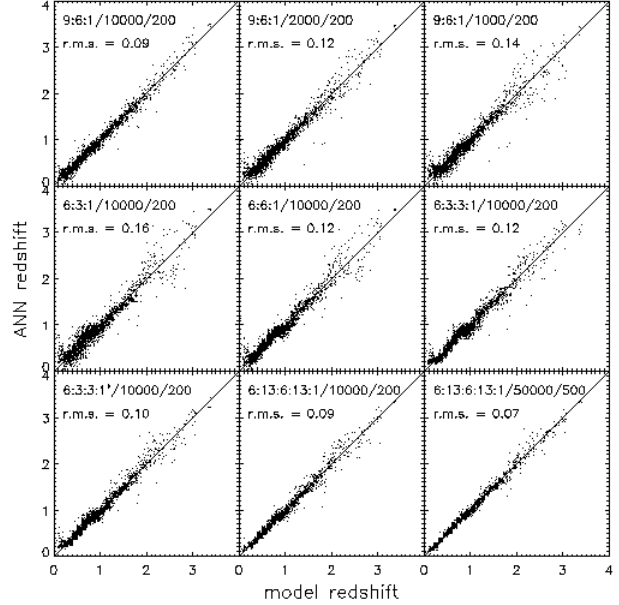


**Figure 3.** Photometric redshift versus model redshift comparisons on the testing set for several network architectures and training set sizes. The format of the labelling is architecture/ $N_{\text{train}}/N_{\text{iter}}$ , where  $N_{\text{train}}$  is the size of the training set and  $N_{\text{iter}}$  is the number of training iterations. The upper three panels compare training set sizes 10000, 2000 and 1000 using a 9:6:1 architecture (*UBVRIZJHK* as inputs) and 200 training iterations. The next five panels compare various architectures taking only 6 inputs (*UBVRIH*) with a fixed training set size (10000) and number of training iterations (200). The panel in the lower right is for the 6:13:6:13:1 architecture with a training set of size 50000 and 500 training iterations. Note that the 6:3:3:1\* architecture has every layer connected to every other layer rather than just consecutive layers connected as in the 6:3:3:1 architecture. The quantization at 0.1 intervals in  $z$ , visible especially in the lower right panel, is due to poor redshift-space resolution in the colour grid used to determine galaxy colours in the semi-analytic model.

## SIMULATED CATALOGUES

### 5.1 Adding photometric noise

To simulate a real galaxy survey, photometric noise was added to the  $H < 22$ , *UBVRIH* catalogue, simulating  $5\sigma$  magnitude limits of  $U = 25.1$ ,  $B = 26.6$ ,  $V = 26.1$ ,  $R = 25.6$ ,  $I = 24.7$  and  $H = 20.5$  (typical of current and future large surveys aimed at studying large-scale structure at high redshifts – e.g. the LCIR Survey, Firth et al. 2001). An extra 0.05 mags r.m.s. error term was included to simulate seeing variations, zeropoint inaccuracies and other sources of photometric errors.  $H < 20.5$  and  $H < 21.5$  ‘noisy’ samples were drawn from this catalogue. In addition ‘noiseless’  $H < 20.5$  and  $H < 21.5$  samples were drawn from the original catalogue. The magnitudes in each catalogue were normalized to the range  $[0, 1]$  using the procedure described above, where the mean magnitudes in each filter were derived from the ‘noiseless’  $H < 20.5$  and  $H < 21.5$  catalogues respectively (the exact form of the normalization is unimportant provided the same normalization is used for both training the ANN and using the ANN). Four 6:13:6:13:1 ANNs were gen-

**Table 2.** The mean and r.m.s. in  $\Delta_z = z_{\text{model}} - z_{\text{phot}}$  for various network architectures, training set sizes  $N_{\text{train}}$ , and number of training iterations  $N_{\text{iter}}$ . The 9:... architectures take 9 inputs (*UBVRIZJHK*) while the 6:... architectures take 6 inputs (*UBVRIH*). In general the nodes in each layer are connected to every node in the adjacent layers only, but in the 6:3:3:1\* architecture all the layers are interconnected. For science applications, a large number of training iterations should be used to ensure convergence, and several different initial random seeds should be investigated.

network architecture	$N_{\text{weights}}$	$N_{\text{train}}$	$N_{\text{iter}}$	mean $\Delta_z$	r.m.s. in $\Delta_z$
9:6:1	67	10000	400	-0.005	0.087
9:6:1	67	10000	200	-0.004	0.088
9:6:1	67	10000	100	-0.005	0.106
9:6:1	67	10000	50	-0.003	0.125
9:6:1	67	20000	200	-0.003	0.085
9:6:1	67	10000	200	-0.004	0.088
9:6:1	67	5000	200	-0.006	0.110
9:6:1	67	2000	200	-0.005	0.120
9:6:1	67	1000	200	-0.009	0.141
9:3:1	34	10000	200	-0.007	0.130
9:3:1	34	10000	50	-0.007	0.211
9:3:1	34	2000	200	-0.004	0.151
9:3:1	34	2000	50	0.003	0.226
6:3:1	25	10000	200	-0.002	0.159
6:3:1	25	5000	200	-0.007	0.160
6:3:1	25	10000	100	-0.006	0.177
6:6:1	49	10000	200	-0.007	0.123
6:6:1	49	5000	200	-0.005	0.131
6:6:1	49	10000	100	-0.004	0.149
6:13:6:13:1	280	50000	500	-0.003	0.069
6:13:6:13:1	280	10000	200	0.000	0.087
6:3:3:1	37	10000	200	-0.001	0.118
6:3:3:1*	64	10000	200	-0.003	0.101

erated using the two magnitude limits and the ‘noisy’ and ‘noiseless’ samples as training sets, with 200 training iterations and a training set size of 10000. The accuracy of each when run on the ‘noiseless’ and ‘noisy’ samples are listed in Table 3. For a ‘noiseless’/‘noisy’ testing set, the accuracy is better when using the ANN trained on respectively the ‘noiseless’/‘noisy’ training set. This is not really surprising but it does confirm that it is important not to use a spectroscopic training set that has different noise characteristics to the testing set. In addition there are small but not insignificant mean offsets in  $\Delta_z = z_{\text{model}} - z_{\text{phot}}$  when an ANN trained on a set with different noise characteristics is used. The r.m.s. error is lowest for the ‘noiseless’ catalogues and, of the ‘noisy’ catalogues, it is lower for the brighter ( $H < 20.5$ ) catalogue.

## 5.2 Comparisons with hyperz

Fig. 4 compares the ANN results for the ‘noisy’  $H < 20.5$  and  $H < 21.5$  samples when trained on the ‘noisy’ training sets. The r.m.s. in  $\Delta_z$  are respectively 0.14 and 0.18 over the redshift range  $0 < z < 3.5$ . Of course, the performance depends entirely on the particular set of filters and limiting magnitudes so, for comparison, the results of the template-fitting code **hyperz**<sup>†</sup> (Bolzonella, Miralles & Pelló 2000) are also shown (using the 8 synthetic Bruzual & Char-

**Table 3.** Comparisons of the mean and r.m.s. in  $\Delta_z = z_{\text{model}} - z_{\text{phot}}$  for  $H < 20.5$  and  $H < 21.5$  ‘noiseless’ and ‘noisy’ samples when using ANNs trained on either ‘noiseless’ or ‘noisy’ training sets. A 6:13:6:13:1 network architecture was used, with a training set of 10000 and 200 training iterations.

training set	‘noiseless testing set’		‘noisy testing set’	
	$\Delta_z$ mean	$\Delta_z$ r.m.s.	$\Delta_z$ mean	$\Delta_z$ r.m.s.
$H < 20.5$				
‘noiseless’	0.003	0.071	-0.002	0.176
‘noisy’	0.016	0.090	0.004	0.141
$H < 21.5$				
‘noiseless’	-0.002	0.071	-0.051	0.331
‘noisy’	0.028	0.133	0.008	0.182

lot 1993 GISSEL’98 evolving templates, that are distributed with **hyperz**, and dust extinction  $A_V$  in the range 0.0–1.2). The **hyperz** results are comparable but slightly worse. Formally the r.m.s. are 0.26 and 0.33 for  $H < 20.5$  and  $H < 21.5$  respectively, but these high values are due more to the small number of complete misidentifications – against which the ANNs seem to be particularly robust – than to a general increased scatter. However, as a further comparison the scatter measured by the half-ranges of the central 68 per cent of  $\Delta_z$  values are 0.03 and 0.03 for the ANNs and 0.11 and 0.14 for **hyperz** for  $H < 20.5$  and  $H < 21.5$  respectively.

It may be argued that **hyperz** is at a disadvantage here

<sup>†</sup> <http://webast.ast.obs-mip.fr/hyperz/>

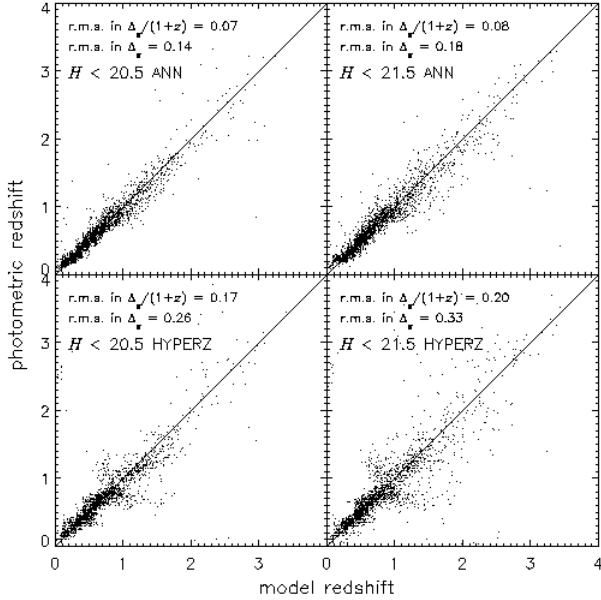


**Figure 4.** A comparison of ANN and `hyperz` photometric redshift errors  $\Delta_z = z_{\text{model}} - z_{\text{phot}}$  on a semi-analytic model catalogue. Photometric noise has been added to mimic  $5\sigma$  magnitude limits of  $U = 25.1$ ,  $B = 26.6$ ,  $V = 26.1$ ,  $R = 25.6$ ,  $I = 24.7$  and  $H = 20.5$ . The ANNs have 6:13:6:13:1 architectures and were trained on similar noisy samples of size 10000 with 200 training iterations. Eight Bruzual & Charlot GISSSEL’98 evolving SEDs were used as templates in `hyperz` with  $A_V$  in the range 0.0–1.2.

relative to the ANNs since the ANN training and testing sets are based on the same spectral models while `hyperz` is trying to fit a different set of templates. For a real data set, `hyperz` – like all template-fitting methods – could still suffer from template mismatches while the ANNs automatically fit the data. Synthetic templates were used in `hyperz` for the above comparison since synthetic templates, albeit from a different source, are used in the semi-analytic model. However when using `hyperz` on real data sets, empirical SEDs, such as the four Coleman et al. (1980, CWW) SEDs – E, Sbc, Scd and Im – distributed with the `hyperz` code, often produce better results. It is possible that the four CWW templates are a closer match to real galaxy SEDs than the eight GISSSEL’98 evolving templates are to the semi-analytic model SEDs. Therefore as a further comparison, which maximally favours `hyperz`, the *UBVRIH* photometry for each galaxy in the semi-analytic model was replaced by *UBVRIH* photometry for the best-fitting (using rest-frame  $B-I$  colour) CWW template SED at the same model redshift. Noise was added to the new photometry as described above and  $H < 20.5$ ,  $H < 21.5$  catalogues were reselected. A new ANN was made for each magnitude limit, using noisy training sets. Fig. 5 compares the two new ANNs with `hyperz`. The formal r.m.s. in  $\Delta_z = z_{\text{model}} - z_{\text{phot}}$  are 0.15 and 0.20 for the ANNs and 0.12 and 0.28 for `hyperz` for  $H < 20.5$  and  $H < 21.5$  respectively, while the half-width of the central 68 per cent  $\Delta_z$  values are 0.02, 0.03 (for the ANNs) and 0.04, 0.06 (`hyperz`). Hence even for this case maximally favouring `hyperz`, the ANNs perform at least as well as template-fitting and rather better on the fainter and noisier sample.

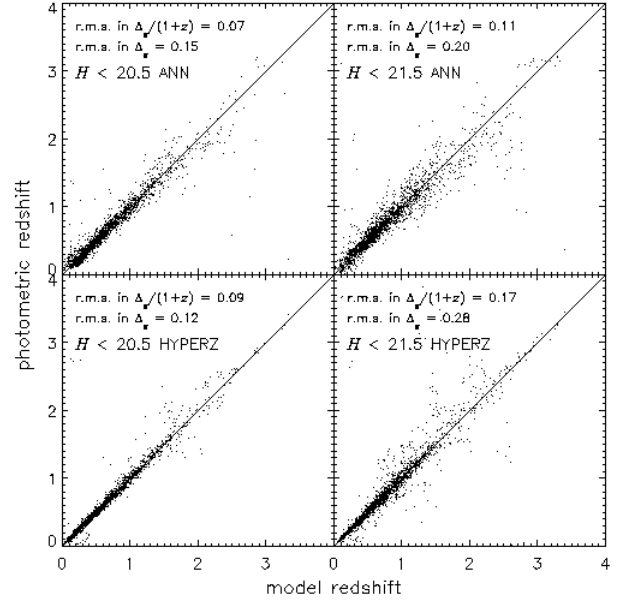


**Figure 5.** A comparison of ANN and `hyperz` photometric redshift errors  $\Delta_z = z_{\text{model}} - z_{\text{phot}}$  on a semi-analytic model catalogue in which the photometry for each model galaxy has been replaced by the photometry of the best-fitting of four empirical CWW template spectra (E, Sbc, Scd or Im) at the same redshift. Photometric noise was then added to mimic  $5\sigma$  magnitude limits of  $U = 25.1$ ,  $B = 26.6$ ,  $V = 26.1$ ,  $R = 25.6$ ,  $I = 24.7$  and  $H = 20.5$ . The ANNs have 6:13:6:13:1 architectures and were trained on similar noisy samples of size 10000 with 200 training iterations. The 4 CWW SEDs themselves were used in `hyperz`.

### 5.3 Scatter due to photometric errors

It is also of interest to see what the distribution of estimated redshifts is for a particular galaxy, as a result of random photometric errors. Random noise was added, as described above, to a selection of individual model galaxies, with 1000 random simulations per galaxy. Then redshifts were estimated using the above previously trained ANNs. Fig. 6 plots histograms of the estimated redshifts for each original galaxy. The width of the  $P(z)$  distribution increases for fainter galaxies but a more pronounced trend is that it increases for galaxies at higher redshifts. There are fewer training galaxies at high redshifts which means that (a) the network weights are less constrained than at lower redshifts, and (b) the training process gives more weight to improving the accuracy for the majority of galaxies at low redshifts at the expense of accuracy at high redshifts. In all the illustrated cases the  $P(z)$  histograms easily encompasses the true redshift with no significant outliers.

### 5.4 Spectral type classification

One can also use ANNs to determine spectral type (independently of redshift) provided, as emphasized above, the training set is representative in terms of both spectral types *and* redshifts (and hence galaxy colours). As in §5.2, the photometry for each semi-analytic model galaxy was replaced by that for the best-fitting CWW template SED at the same model redshift. Then simulated photometric noise was added

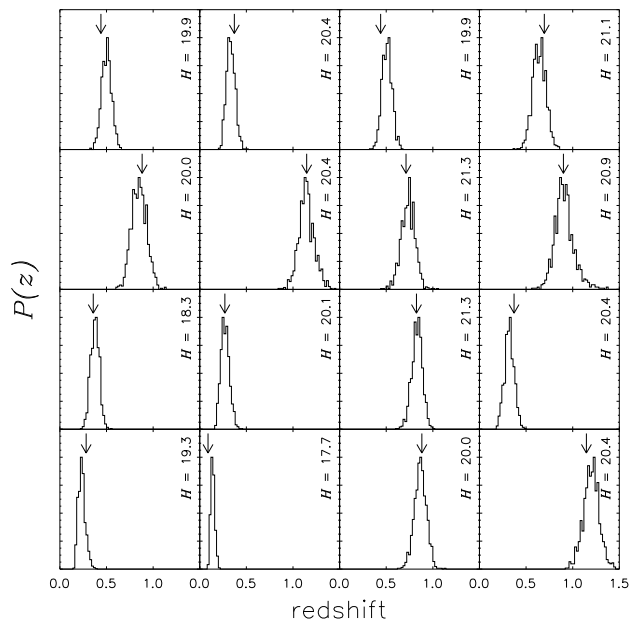


**Figure 6.** Eight galaxies were selected from each of the  $H < 20.5$  and  $H < 21.5$  ‘noiseless’ catalogues. Random photometric noise was added simulating  $5\sigma$  limiting magnitudes  $U = 25.1$ ,  $B = 26.6$ ,  $V = 26.1$ ,  $R = 25.6$ ,  $I = 24.7$  and  $H = 20.5$ , with 1000 simulations per initial galaxy. The plots shows histograms (one for each of the original 16 galaxies) of the redshifts estimated with the ANNs previously trained on the full ‘noisy’  $H < 20.5$  and  $H < 21.5$  training sets (see text) respectively. The 8 panels on the left were selected from the  $H < 20.5$  catalogue while the 8 panels on the right were selected from the  $H < 21.5$  catalogue. The arrows indicate the true (model) redshift of each galaxy and the  $H$  magnitude of each original galaxy is also indicated.

and  $H < 20.5$  and  $H < 21.5$  catalogues were selected. The best-fitting CWW spectral types E, Sbc, Scd and Im give the desired output on which the network is trained.

One possible architecture is to have four output nodes – one for each CWW spectral type. When training, the desired output would be 1 for the output node corresponding to the correct type and 0 for the other three nodes. When a galaxy of unknown spectral type is run through the ANN, the output in each node may be treated as a probability for the galaxy being of the corresponding type, and the galaxy would be assigned the type for which the probability is greatest (see e.g. Storrie-Lombardi et al. 1992; Lahav et al. 1996). Alternatively, since galaxy spectral types roughly follow a sequence (e.g. Connolly et al. 1995a), a network with a single output node may be utilized. Using this approach, the CWW spectral types E, Sbc, Scd and Im (at any redshift) were coded by the desired output types 0.2, 0.4, 0.6 and 0.8 respectively. The input magnitudes were normalized to the range  $[0, 1]$  as above. Once again a 6:13:6:13:1 architecture, 10000 training objects and 200 training iterations were used.

The ANN results are displayed in Fig. 7. The ANN spectral types agree very well with the original CWW spectral types – the r.m.s. in  $\Delta_{\text{SED}}$  on the above scale are 0.03 and 0.04 for the  $H < 20.5$  and  $H < 21.5$  samples respectively.

Similarly `hyperz` may be used to attempt to recover the input CWW spectral type from the noisy photometry. Spectral type is a discrete variable for `hyperz` but continu-

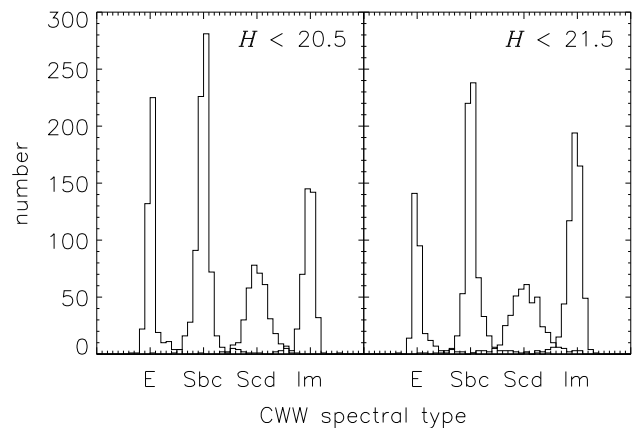


**Figure 7.** Histograms of spectral type estimated with ANNs trained and tested on  $H < 20.5$  and  $H < 21.5$  ‘noisy’  $UBVR IH$  catalogues. The ANNs spectral type output is a continuous variable while the training spectral types CWW E, Sbc, Scd and Im are discrete variables at the indicated positions. The ANN spectral types agree very well with the true spectral types.

ous for the ANN (the latter being the more useful statistic for real data sets). To compare these, the ANN results were discretized (Table 4). The ANNs and `hyperz` perform comparably well.

## 5.5 Alternative networks

In principle one may design a single ANN with many output nodes (or many ANNs with one output node each) which produce a  $P(z)$  distribution for each input object. An ANN could have, for example, 400 output nodes corresponding to 0.01 steps in redshift from  $z = 0$  to  $z = 4$ . When training, the desired output  $z_k^p$  is 1 for the output node corresponding to the correct redshift and 0 for all other nodes. Running the ANN on a new object will produce 400 outputs in the range  $[0, 1]$  which may be treated as a probability distribution  $P(z)$ . Training such a large ANN would however require extensive computer resources.

One can also take the magnitude errors as ANN input – this allows the ANN to train itself to put less weight on the magnitudes with larger errors. In the simulations this adds no new information since there is a one-to-one correspondence between the magnitude in each filter and the magnitude errors (that is the r.m.s errors, not the actual errors themselves which are random and unknown), so these are not used here, but in a real data set this is not necessarily the case. One can also take other observational input such as image size or surface brightness, morphology and concentration parameters (e.g. see §6).

## 6 PERFORMANCE OF NEURAL NETWORKS

**Table 4.** Comparisons of the efficiency with which ANNs and `hyperz` recover galaxy spectral types for  $H < 20.5$  and  $H < 21.5$  semi-analytic model *UBVRIH* photometric catalogues with  $5\sigma$  limiting magnitudes  $U = 25.1$ ,  $B = 26.6$ ,  $V = 26.1$ ,  $R = 25.6$ ,  $I = 24.7$  and  $H = 20.5$ .

estimated SED	hyperz				ANN			
	E	Sbc	Scd	Im	E	Sbc	Scd	Im
$H < 20.5$								
true SED								
E	428	1	0	0	425	4	0	0
Sbc	9	743	1	0	1	741	11	0
Scd	0	3	383	0	0	5	374	7
Im	0	0	9	423	1	0	8	423
$H < 21.5$								
true SED								
E	298	2	1	1	291	11	0	0
Sbc	15	651	9	1	4	656	16	0
Scd	0	17	395	5	0	14	374	29
Im	0	0	40	565	0	0	10	595

## ON SDSS DATA

The Sloan Digital Sky Survey<sup>‡</sup> (SDSS; York et al. 2000) consortium have now publicly released more than 50000 spectroscopic redshifts along with *ugriz* photometry and various image morphological parameters. These provide an excellent opportunity to test ANNs on real data (see also Sowards-Emmerd et al. 2000 for a polynomial-fitting approach). 23000 objects were selected from the SDSS public data set using the following criteria: (1) the spectroscopic redshift confidence must be greater than 0.95 and there must be no warning flags, (2)  $r < 17.5$ . Stars were left in with the galaxies but at these magnitudes they could have been fairly robustly removed using image morphology. The resulting catalogue was almost entirely limited to  $z < 0.5$ . The order was randomized, the parameters were normalized to the range  $[0, 1]$ , and non-overlapping training (15000) and testing (8000) sets were selected. Two ANNs were generated. One, with the architecture 5:11:5:11:1, inputting *ugriz* photometry, and the other, with the architecture 8:17:8:17:1, inputting *ugriz* photometry and the SDSS pipeline star/galaxy classifier (‘type’) and Petrosian 50 per cent and 90 per cent  $r$ -band flux radii,  $r_{50}$  and  $r_{90}$ . The networks were trained with 200 training iterations.

Fig. 8 compares the ANN redshifts with spectroscopic redshifts for the testing sets. The r.m.s. in  $\Delta_z$  are 0.023 and 0.022 for the 5:11:5:11:1 and 8:17:8:17:1 networks respectively, while the mean offsets are 0.001 and 0.000. These

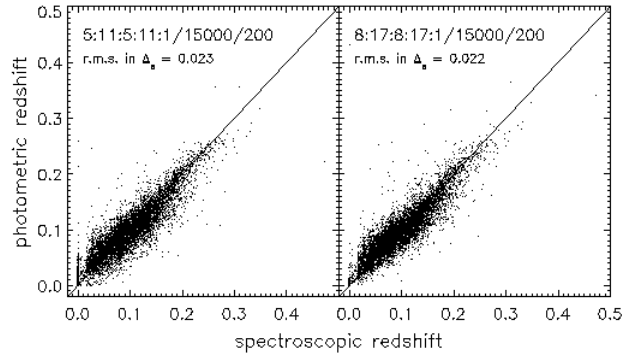


**Figure 8.** A comparison of photometric and spectroscopic redshifts using SDSS public data. Two ANNs were trained on a training set of size 15000 taking as input *ugriz* photometry (5:11:5:11:1 architecture, left) and *ugriz* photometry, SDSS star/galaxy classifier and Petrosian 50 and 90 per cent  $r$ -band flux radii (8:17:8:17:1 architecture, right). 200 training iterations were used. The ANNs were tested on a separate testing set of size 8000 (plotted).

results did not significantly improve when 500 training iterations were used and did not significantly change when different random seeds were used. They are easily as good as, and probably better than, the best results that template-fitting photometric redshift methods can produce. There are also very few outliers. The spike at  $z = 0$  in the 5:11:5:11:1 network results is due to misidentified stars. In the 8:17:8:17:1 network the addition of morphological parameters largely removes this feature.

While 15000 training objects were used for the above networks, one can still do fairly well with much smaller training set sizes. The 5:11:5:11:1 and 8:17:8:17:1 architectures have respectively 204 and 468 weights (free parameters) and significantly greater training set sizes are required in order that they be well-determined. Therefore to investigate a wide range of training set sizes on an equal footing, simpler architectures – viz. 5:5:1 and 8:8:1 (with 36 and 81 weights respectively) – were used. Fig. 9 shows the effect of training set size on the r.m.s. in  $\Delta_z$ . Even for a training set of size 200, the r.m.s. is only 0.029 for the 8:8:1 architecture.

<sup>‡</sup> Funding for the creation and distribution of the SDSS Archive has been provided by the Alfred P. Sloan Foundation, the Participating Institutions, the National Aeronautics and Space Administration, the National Science Foundation, the U.S. Department of Energy, the Japanese Monbukagakusho, and the Max Planck Society. The SDSS Web site is <http://www.sdss.org/>. The Participating Institutions are The University of Chicago, Fermilab, the Institute for Advanced Study, the Japan Participation Group, The Johns Hopkins University, the Max-Planck-Institute for Astronomy (MPIA), the Max-Planck-Institute for Astrophysics (MPA), New Mexico State University, Princeton University, the United States Naval Observatory, and the University of Washington.



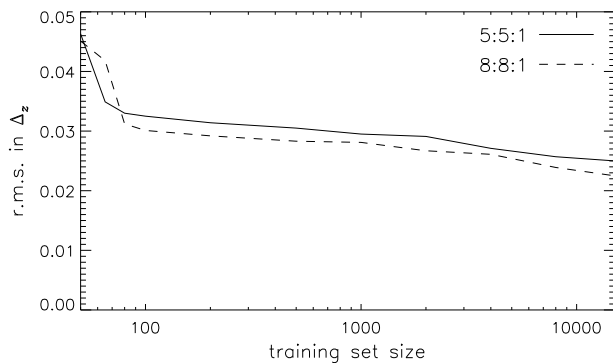


**Figure 9.** Photometric redshift accuracy as a function of training set size for SDSS data. Results are given for two ANNs, taking as input *ugriz* photometry (5:5:1 architecture) and *ugriz* photometry, SDSS star/galaxy classifier and Petrosian 50 and 90 per cent *r*-band flux radii (8:8:1 architecture). 500 training iterations were used. The ANNs were tested on a separate testing set of size 8000 and the r.m.s. in  $\Delta z = z_{\text{model}} - z_{\text{phot}}$  is plotted. When the training set size is of order the number of weights in the network (36 and 81 respectively), the accuracy deteriorates rapidly. For comparison, the r.m.s. of the redshift distribution of the 8000 objects in the testing set is 0.054. This is the r.m.s. that could be achieved by fitting a single value to the data.

Very small training sets do however lead to loss of accuracy for rare objects (e.g. the high redshift tail).

## 7 CONCLUSIONS

ANNs can produce photometric redshift accuracies that are comparable to or better than template-fitting procedures (particularly in the case of poor S/N). However they do rely on large and representative training samples and an ANN is only applicable to the particular survey filters and redshift range upon which it has been trained. For large photometric/spectroscopic surveys, such as the SDSS and future deeper surveys such as DEEP2<sup>§</sup> and the VIRMOS-VLT Deep Survey<sup>¶</sup> (VVDS; Le Fèvre et al. 2000), where large spectroscopic samples are available, it seems that ANNs offer some significant advantages over previous approaches. The VVDS, for example, is expected to include  $> 100000$  redshifts to  $I_{AB} = 22.5$ ,  $> 40000$  redshifts to  $I_{AB} = 24$  and  $> 1000$  redshifts to  $I_{AB} = 25$ , providing ample training set sizes for the complementary deep imaging in *UBVRICK<sub>s</sub>* to  $I_{AB} = 25$  (similar to the limits used in §5).

With careful modelling of photometric errors and some loss in the Bayesian statistics, bright spectroscopic samples may also be extrapolated to provide training sets for fainter photometric samples.

In addition, ANNs may also be used where spectroscopic redshifts are unavailable, by utilizing a simulated catalogue (e.g. semi-analytic model) as a training set. By using theoretical SEDs in the training set, this method has all the disadvantages and advantages of standard template-fitting, but it also has the extra advantages (i) the ‘template’ SEDs

include a (more or less) realistic distribution of *complex* star formation histories, dust modelling and metallicities etc., giving fully Bayesian statistics, and (ii) the weights applied to different filters (and non-linear combinations thereof) may be more optimal than simple  $\chi^2$ -weighting.

To conclude, while photometric redshifts may be used to good effect in pioneering studies of new populations of objects, spectroscopic confirmation will always be necessary to obtain truly robust scientific results. Instead the real power of photometric redshifts lies in extending small very resource-intensive faint spectroscopic surveys to much larger fields-of-view and sample sizes. That is to say, the area where photometric redshifts can best be used for robust and useful scientific gains is in the training-set regime and, if accuracies of  $\sim 0.02$ – $0.07$  in redshift can be achieved at low and high redshifts, as indicated in this paper, then photometric redshifts will be a very powerful tool indeed in future large surveys.

## ACKNOWLEDGMENTS

We are grateful to B. D. Ripley for providing the ANN training code, Avi Naim for related programmes and advice and Richard Ellis and Richard McMahon for useful discussions. AF was supported by Trinity College, Cambridge, an Isaac Newton Studentship, and an L. B. Wood Travelling Scholarship during this work.

## REFERENCES

- Allende Prieto C., Rebolo R., López R. J. G., Serra-Ricart M., Beers T. C., Rossi S., Bonifacio P., Molaro P., 2000, *AJ*, 120, 1516
- Andreone S., Gargiulo G., Longo G., Tagliaferri R., Capuano N., 2000, *MNRAS*, 319, 700
- Bailer-Jones C. A. L., Irwin M., von Hippel T., 1998, *MNRAS*, 298, 361
- Baum W. A., 1962, *Problems of Extragalactic Research*, IAU Symposium No. 15, 390
- Benitez N., 1998, *Abstracts of the 19th Texas Symposium on Relativistic Astrophysics and Cosmology*, eds, J. Paul, T. Montmerle, E. Aubourg
- Bertin E., Arnouts S., 1996, *A&AS*, 117, 393
- Bolzonella M., Miralles J.-M., Pelló R., 2000, *A&A*, 363, 476
- Brunner R. J., Szalay A. S., Connolly A. J., 2000, *ApJ*, 541, 527
- Bruzual A. G., Charlot S., 1993, *ApJ*, 405, 538
- Cole S., Aragón-Salamanca A., Frenk C., Navarro J., Zepf S., 1994, *MNRAS*, 271, 781
- Coleman G. D., Wu C.-C., Weedman D. W., 1980, *ApJS*, 43, 393
- Connolly A. J., Szalay A. S., Bershady M. A., Kinney A. L., Calzetti D., 1995a, *AJ*, 110, 1071
- Connolly A. J., Csabai I., Szalay A. S., Koo D. C., Kron R. G., Munn J. A., 1995b, *AJ*, 110, 2655
- Connolly A. J., Szalay A. S., Brunner R. J., 1998, *ApJ*, 499, L125
- Devriendt J. E. G., Guiderdoni B., Sadat R., 1999, *A&A*, 350, 381
- Fernández-Soto A., Lanzetta K. M., Yahil A., 1999, *ApJ*, 513, 34
- Fernández-Soto A., Lanzetta K. M., Chen H.-W., Pascarelle S. M., Yahata N., 2001, *ApJS*, 135, 41
- Firth A. E. et al., 2001, *astro-ph/0108182*
- Firth A. E., 2002, Ph.D. Thesis, Univ. Cambridge, U.K.
- Fontana A., D’Odorico S., Poli F., Giallongo E., Arnouts S., Cristiani S., Moorwood A., Saracco P., 2000, *AJ*, 120, 2206

<sup>§</sup> <http://astron.berkeley.edu/~marc/deep/>

<sup>¶</sup> <http://www.astrsp-mrs.fr/virmos/>

- Gwyn S. D. J., Hartwick F. D. A., 1996, *ApJ*, 468, L77  
Hogg D. W. et al., 1998, *AJ*, 115, 1418  
Kauffmann G., White S., Guiderdoni B., 1993, *MNRAS*, 264, 201  
Lahav O., Naim A., Sodr e L. Jr., Storrie-Lombardi M. C., 1996, *MNRAS*, 283, 207  
Le F evre et al., 2000, in Clowes R. G., Adamson A. J., Bromage G. E., eds, *ASP Conf. Ser. Vol. 232, New Era of Wide-Field Astronomy*. Astron. Soc. Pac., San Francisco, p. 449  
Massarotti M., Iovino A., Buzzoni A., 2001a, *A&A*, 368, 74  
Massarotti M., Iovino A., Buzzoni A., Valls-Gabaud D., 2001b, *A&A*, 380, 425  
Sheth R. K., Tormen G., 1999, *MNRAS*, 308, 119  
Somerville R. S., 1997, PhD Thesis, Univ. California, Santa Cruz  
Somerville R. S., Primack, J. R., 1999, *MNRAS*, 310, 1087  
Somerville R. S., Primack J. R., Faber S. M., 2001, *MNRAS*, 320, 504  
Sowards-Emmerd D., Smith J. A., McKay T. A., Sheldon E., Tucker D. L., Castander F. J., 2000, *AJ*, 119, 2598  
Storrie-Lombardi M. C., Lahav O., Sodr e L. Jr., Storrie-Lombardi L. J., 1992, *MNRAS*, 259, 8  
Teplitz H. I., Hill R. S., Malumuth E. M., Collins N. R., Gardner J. P., Palunas P., Woodgate B. E., 2001, *ApJ*, 548, 127  
Weaver W. B., 2000, *ApJ*, 541, 298  
Weymann R. J., Storrie-Lombardi L., Sawicki M., Brunner R. J., eds, 1999, *ASP Conf. Ser. Vol. 191, Photometric Redshifts and High Redshift Galaxies*, Astron. Soc. Pac., San Francisco  
York D. G. et al., 2000, *AJ*, 120, 1579

This paper has been produced using the Royal Astronomical Society/Blackwell Science L<sup>A</sup>T<sub>E</sub>X style file.